Comprehensive Study of the Formation and Reaction of a Tethered N-Hydroxysulfosuccinimidyl Ester Used to Covalently Tether Proteins to Surfaces

Alice A. Deckert,* Kelley A. Anderson, Kate M. Mullaugh, and Christine Delaney

Allegheny College, Department of Chemistry, Meadville, Pennsylvania 16335

Received: May 26, 2004; In Final Form: July 20, 2004

A fundamental understanding of surface-reaction kinetics and mechanisms is essential to making progress on rational design of complex surface architectures used in applications as varied as biosensor devices and organic electronic devices. We present recent progress on the understanding of the carbodiimide coupling reaction frequently used to form a surface-tethered active N-hydroxysulfosuccinimide ester and the subsequent substitution of the active ester with various nucleophiles in solution. These studies were carried out using surface-enhanced Raman spectroscopy (SERS) and show that the carbodiimide coupling reaction is first order in carbodiimide concentration and zero order in N-hydroxysulfosuccinimide concentration. This reaction proceeds with a second-order rate constant of 0.062 $mM^{-1}s^{-1}$ at about 20 °C. The tethered active ester was then reacted with histidine or glucose oxidase. The reaction with histidine was found to be first order in the histidine solution concentration, indicating a simple S_N2 reaction mechanism with a second-order rate constant of 0.010 $mM^{-1}s^{-1}$. The reaction with glucose oxidase had more complicated kinetics that were consistent with the formation of a surface bound acylium ion intermediate.

Introduction

Investigations of the immobilization of proteins and other biologically relevant molecules to solid substrates have increased dramatically during the past decade.[1−4] Specifically, the possibility of forming biosensors from biomolecules covalently bound to suitable organic thin films is of increasing interest and numerous studies have addressed some of the major issues inherent in covalent immobilization of large molecules to surfaces.[4−15] This interest is sparked, in part, by the inherent stability of covalent bonds.[5,6]

Many reaction schemes have been developed to attach biological recognition systems to suitable surfaces. All of these methods have their own advantages and disadvantages and very few of them are understood in any fundamental kinetic and mechanistic way. Some covalent immobilization techniques provide strong bonds for robust devices but require multiple fabrication or synthesis steps.[13−17] Physical adsorption techniques are general and simple but do not always allow for control of protein coverage or orientation and result in less robust devices due to protein leaching.[18−20] Several strategies have been developed that employ strong interactions between a protein and a surface-bound species that result in robust devices and allow for control of protein coverage, but require protein engineering.[21−23] Strong ligand−acceptor interactions can be employed to fabricate robust devices but can often only be applied to a limited set of recognition systems.[24−26]

Unfortunately, both the development of general methods and the application of existing methods for protein immobilization are hampered by a lack of basic understanding of the reactions and interactions that occur at thin-film and matrix surfaces. To date, very few comprehensive studies of the kinetics and mechanism of covalent reactions between proteins and thin films have been carried out.[7−9] The reaction of a carbodiimide and a N-hydroxysuccinimide with a tethered carboxylic acid has been used by many groups to form the active tethered N-hydroxysuccinimide ester.[3,11,25] This active ester can be further reacted with a protein in solution resulting in covalent attachment of the protein through a peptide bond.[25]

We have studied the formation and reaction of a tethered N-hydroxysulfosuccinimide ester in detail using surface enhanced Raman spectroscopy (SERS) and present those results here. We begin with an overview of the SERS technique and then examine the kinetics of formation of the active ester. Finally, we discuss the results of the substitution reactions involving histidine and glucose oxidase.

Surface Enhanced Raman Spectroscopy (SERS)

Several techniques have been developed recently that allow sensitive detection of surface species in real time. This has opened up the possibility of monitoring reactions in real time and thus obtaining a fundamental kinetic and mechanistic understanding of surface reactions. One such technique uses the enhancement of the Raman signal for molecules attached to a gold or silver surface.

The enhancement of the Raman signal when molecules are adsorbed to a metal surface (most notably gold or silver) has been well studied.[27−28] This effect, which is generally believed to be due to the interaction of surface plasmons with the Raman scattering process, can enhance the normally weak Raman signal by six orders of magnitude.[28] In addition to being very surface sensitive, SERS provides specific molecular information in the form of vibrational frequencies for adsorbed species. So far, this technique has been underused for the real-time study of surface reaction kinetics.

The SERS technique can be used to study species on roughened gold and silver surfaces[28] and has also been used to

* To whom correspondence should be addressed. e-mail: adeckert@allegheny.edu, fax: 814-332-2789, phone: 814-332-5329.

10.1021/jp047718b CCC: $27.50
Published on Web 09/09/2004

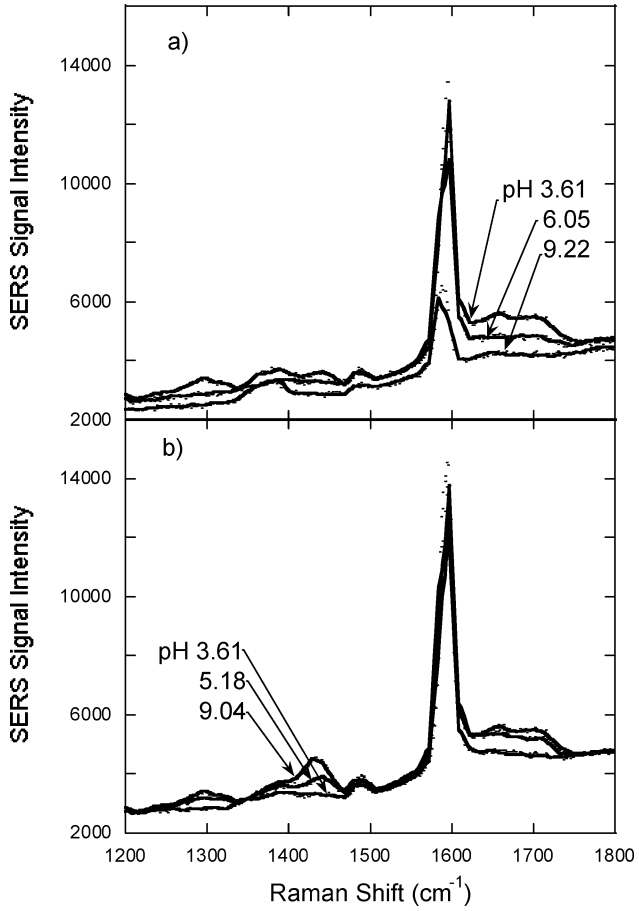

Figure 1. SER spectrum of silver colloids saturated with 4-mercaptobenzoic acid is shown as a function of (a) descending and (b) ascending pH. The Raman scattering signal is enhanced by the aggregation of the colloids as the pH is lowered. The protonation and deprotonation of the carboxylic acid group is clearly evidenced by the change in the scattering signal near 1700 and 1450 cm^{-1}. Note the isosbestic point around 1330 cm^{-1}.

study species adsorbed to colloidal gold and silver particles.[28] In this work we have used colloidal silver systems. A couple of characteristics of these systems must be taken into account when using SERS to quantify surface coverage.

The enhancement of the SERS signal is very sensitive to the shape and structure of the colloids.[28] Silver colloid solutions with nearly all spherical colloids of a narrow size distribution can be made by a number of different methods.[29] All of these methods result in stable colloids that will tend to aggregate when an adsorbate such as pyridine[28,29] or an alkyl or aryl thiol is added. The degree of aggregation strongly affects the enhancement of the signal and is sensitive to the pH of the solution. Figure 1a shows the SER spectrum of a saturated layer of 4-mercaptobenzoic acid on silver colloids as a function of descending pH. Figure 1b shows the SER spectrum of the same colloid solution as a function of ascending pH.

As the pH is decreased the signal at 1600 cm^{-1} becomes very intense. In addition, there are intensity changes in the 1725, 1300, and 1450 cm^{-1} regions. When the pH is increased, the intensity at 1600 cm^{-1} remains essentially constant, while the intensity near 1725 and 1300 cm^{-1} decreases and the intensity near 1450 cm^{-1} increases. These scattering peaks can be assigned to the protonated carboxylic acid and the deprotonated carboxylate groups. There appears to be an isosbestic point near 1330 cm^{-1} indicating that the Raman scattering signal is linear in carboxylic acid and carboxylate coverage.

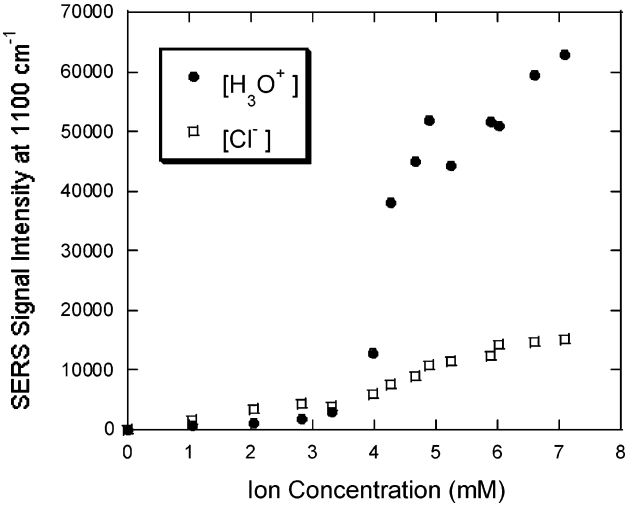

Figure 2. Enhancement of the SERS signal at 1600 cm^{-1} for silver colloids saturated with 4-mercaptobenzoic acid is shown as a function of (●) H_3O^+ concentration and (□) Cl^- concentration. The hydronium ion clearly has a much larger effect on the SERS signal than does the chloride ion.

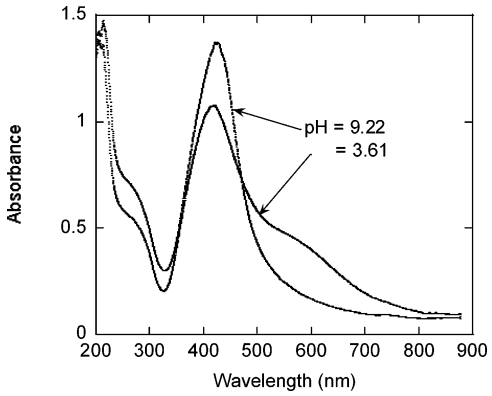

Figure 3. UV−Visible spectrum of the colloid solution at high pH before aggregation and at low pH after aggregation. Note the appearance of the longer wavelength absorbance due to the shift in the plasmon resonance for larger particles.

Chloride ions have also been implicated in the colloid aggregation process.[30,31] Figure 2 shows the intensity of the Raman signal at 1600 cm^{-1} as a function of both the chloride ion concentration (using NaCl(aq) to achieve a given $[Cl^-]$) and the hydronium ion concentration (using HCl(aq) to achieve a given pH). Clearly, the hydronium ion has a much larger effect on the SERS signal than does the chloride ion. The overall negative charge of the carboxylate-saturated colloidal particles result in strong repulsive electrostatic forces that keep the particles apart in solution. However, when the carboxylate group is protonated at low pH, these repulsive electrostatic forces between particles are no longer present. This allows the colloidal particles to aggregate.

The visible spectrum of the colloids is known to change as the degree of aggregation changes.[28] In fact, the solutions change from a clear yellow, through a rosy pink, to a greenish-gray color as the pH is decreased. Figure 3 shows the visible spectrum of the colloid solution at pH 9.22 and 3.61.

Clearly, the aggregation of the colloids is dramatically affected by lowering the pH of the system. In addition, the aggregation seems to be irreversible since the Raman signal intensity and the visible spectrum remain unchanged upon raising the pH from 3 to 9.

SCHEME 1: NHSS Carbodiimide Coupling Reaction

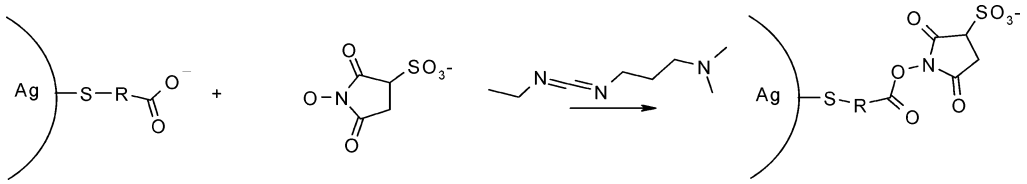

These data have consequences for the quantification of spectral changes due to reactions occurring on the surface of the colloids. Care must be taken so that any reaction that occurs with the organic layer on the colloids does not change the degree of colloid aggregation. The degree of aggregation can easily be monitored using an internal standard, such as a vibration in the adsorbate layer, that does not change during reaction (i.e. Raman shift = 1600 cm^{-1} for the 4-mercaptobenzoic acid layer shown in Figure 1.) In addition, the visible spectrum of the colloid solution is very sensitive to the degree of aggregation and can be used as a further check that spectral changes are due to reaction and not to further enhancement of the SERS signal due to colloid aggregation.

Another consideration in using SERS to study surface reactions is the thickness of the active layer. Since SERS is a near field effect, thicker layers will have far less signal enhancement and the sensitivity of the technique will be reduced.[28] Thus systems must be designed so that the reaction takes place near the silver or gold surface where the spectral changes can be quantified and real-time kinetic information can be derived.

Results and Discussion

Formation of the N-Hydroxysulfosuccinimide Active Ester. We have measured the kinetics of the formation of an active N-hydroxysulfosuccinimde (NHSS) ester on the 4-mercaptobenzoic acid saturated silver colloids. This reaction is shown in scheme 1. The reaction of the NHSS with the surface-bound 4-mercaptobenzoic acid was carried out with various concentrations of 1-[3-(Dimethylamino)propyl]-3-ethylcarbodiimide hydrochloride (EDC) ranging from 0.1 to 0.5 mM for various concentrations of NHSS between 1 and 4 mM. The reaction was followed as a function of time by monitoring the ratio of the height of the scattering peak appearing at 1780 cm^{-1} (which can be attributed to the carbonyl stretches on the succinimide ring system) to the height of the scattering peak at 1600 cm^{-1} (which can be attributed to the phenyl ring system and does not change during the reaction). This peak height ratio increased exponentially in time, as shown in Figure 4. Each of the four NHSS concentrations investigated resulted in the same pseudo-first-order rate constants for each EDC concentration.

SCHEME 2: NHSS Carbodiimide Coupling Mechanism

$$S - RCOOH + EDC \xrightarrow{k_1} S - RCOOHEDC$$

$$S - RCOOHEDC + NHSS \xrightarrow{k_2} S - RCONHSS + urea\ cmpd$$

The pseudo-first-order rate constants, regardless of NHSS concentration, were found to depend linearly on the EDC concentration as shown in Figure 5. The slope of the best-fit line to the data in Figure 5 resulted in a second-order rate constant of 0.062 $mM^{-1}s^{-1}$.

These data are consistent with the reaction mechanism shown in Scheme 2. If the formation of the EDC adduct on the surface (k_1) is rate limiting, there will be no dependence of the overall rate on the NHSS concentration as observed. Quantitatively, the integrated rate equation can be determined subject to the steady-state approximation for the EDC adduct and compared to the experimental data. The integrated rate equation for the appearance of the NHSS ester on the surface is shown in eq 1 where θ_{NHSS} represents the relative coverage of the NHSS ester on the surface.

$$\theta_{NHS} = (1 - e^{-(k1[EDC])t}) \quad (1)$$

The solid lines shown through the data points in Figure 4 are the best fits to eq 1. According to eq 1, the appearance of the NHSS peak should be simple first order with an observed rate constant that is linearly dependent on the EDC concentration. Thus, the slope of the best-fit line in Figure 5 corresponds

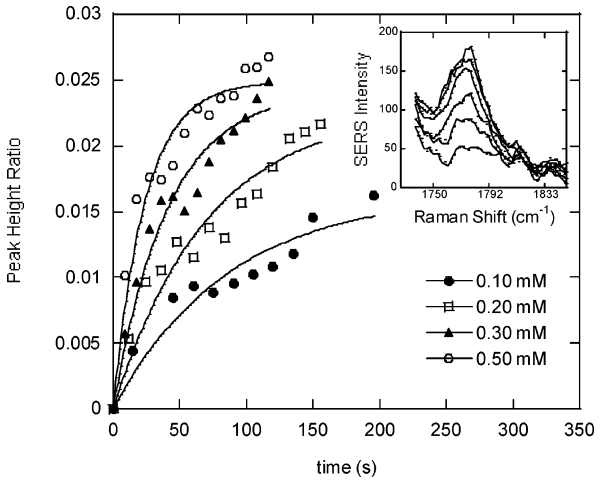

Figure 4. Kinetic profiles for different concentrations of EDC as indicated in the legend. The ratio of the height of the scattering peak at 1780 cm^{-1} to the peak at 1600 cm^{-1} is plotted on the *y*-axis. The solid lines are the best fit to eq 1 in the text. The insert shows the development of the peak at 1780 cm^{-1} over time from 0s to 126 s into the reaction for an EDC concentration of 0.40 mM.

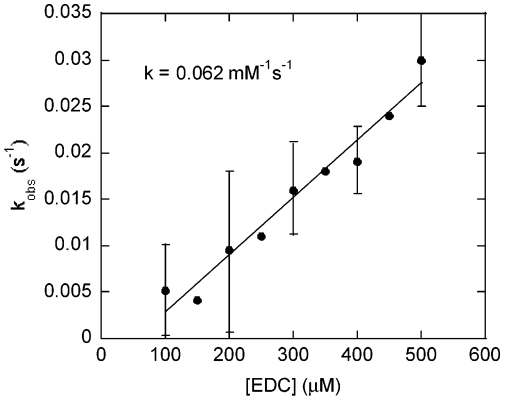

Figure 5. Observed average rate constants determined from the exponential fits to the data shown in Figure 4 are shown as a function of the EDC concentration. Rate constants from each of four NHSS concentrations were averaged. The error bars represent the standard deviation over the four points. Points without error bars were only obtained at one NHSS concentration of 1 mM.

SCHEME 3: Substitution Reaction

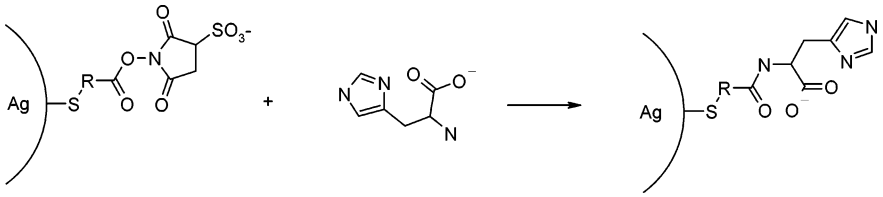

to the second-order rate constant for the formation of the EDC adduct ($k_1 = 0.062$ mM^{-1}s^{-1}).

Attachment of Histidine. The tethered NHSS ester of 4-mercaptobenzoic acid was reacted with histidine to form a peptide bond to the surface. The reaction, shown in Scheme 3, was monitored both by the disappearance of the 1780 cm^{-1} succinimide stretch and by the appearance of increased scattering intensity around 1450 cm^{-1}. The 1450 cm^{-1} region is complicated due to succinimide absorbance in that region and no quantitative data could be obtained. However, the decrease in the 1780 cm^{-1} peak area qualitatively coincided with the increase in peak area at 1450 cm^{-1}. The spectra revealed no change to the 1600 cm^{-1} intensity indicating no signal enhancement due to colloid aggregation. The exponential fits to the disappearance of the 1780 cm^{-1} peak for different concentrations of histidine are shown as solid lines through the data in Figure 6.

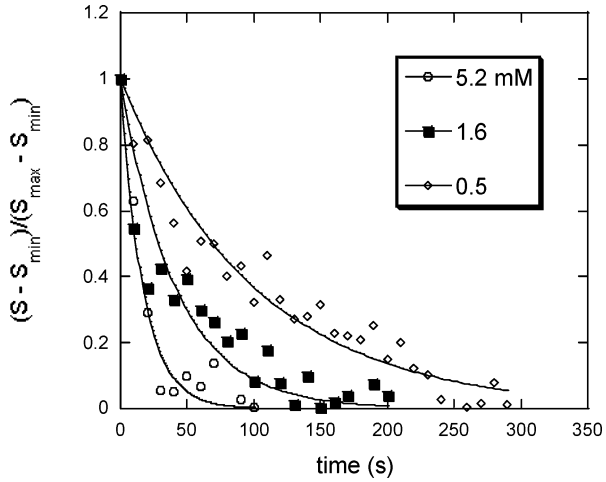

Figure 6. Kinetic profiles for the reaction of histidine with a tethered NHSS ester on the surface of the silver colloids. The normalized area under the scattering peak at 1780 cm^{-1} is shown as a function of time for three different histidine concentrations as indicated in the legend. The solid lines through the data represent the best fit to an exponential decay.

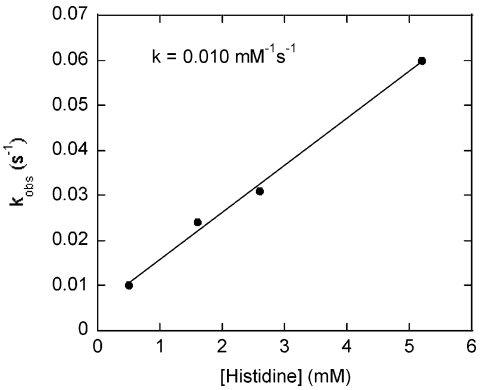

Figure 7. Observed rate constants derived from the best-fit curves to the data shown in Figure 6. The psuedo-first-order rate constants are linear in histidine concentration and the best fit line provides a second-order rate constant of 0.010 mM^{-1}s^{-1}.

The pseudo-first-order rate constants obtained from the fits to the data in Figure 6 are plotted as a function of the histidine concentration in Figure 7. These data are clearly linear and the best-fit line provides a second-order rate constant for the reaction of 0.010 mM^{-1}s^{-1}.

Glucose Oxidase Attachment Studies. The attachment of glucose oxidase to silver colloids saturated with the active NHSS ester of 16-mercaptohexadecanoic acid was studied using SERS. Figure 8 shows a representative graph of the intensity of the 980 cm^{-1} peak (due to glucose oxidase) versus time.

The graphs were fit to a simple exponential association and the value of the decay constant (k_{obs}) obtained from the regression analysis for each glucose oxidase concentration was found to be linear in glucose oxidase concentration as shown in Figure 9.

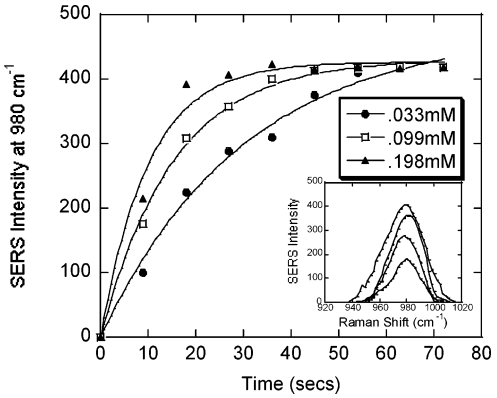

Figure 8. Graph depicts the change in peak height at 980 cm^{-1} monitored with time. The reaction was carried out at a pH of approximately 9.5. Although the GoX stock solution was buffered at pH 7 (phosphate buffer) the colloid solutions were not buffered. The closed circles represent 0.033 mM GoX, the open squares represent 0.099 mM GoX, and the closed triangles represent 0.198 mM GoX. The solid line through the data depicts a fit to a simple exponential association. The insert shows the increase in the GoX peak at 980 cm^{-1} over time.

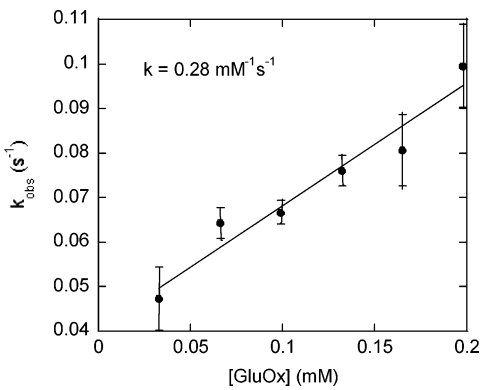

Figure 9. k_{obs} obtained from the fits represented in Figure 8 is graphed against the concentration of GoX. The solid line represents the linear best fit to the data. The error bars indicate ±1 standard deviation over three trials.

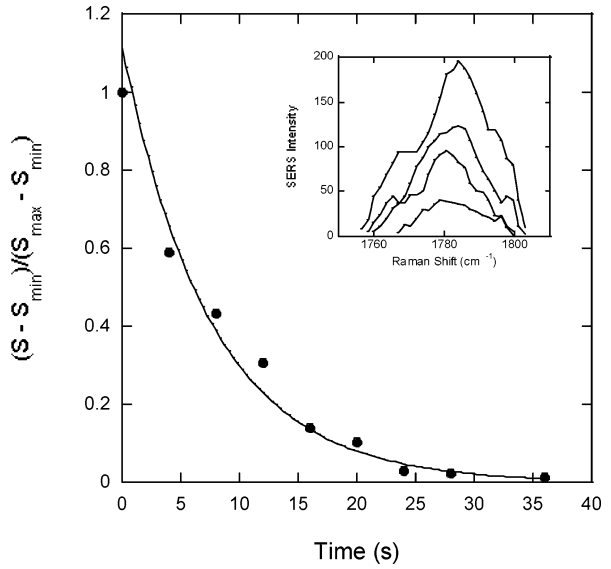

Figure 10. Peak intensity of the NHSS peak as a function of time. The circles represent the peak intensity for a [GoX] = 0.198 mM. Only one representative curve is shown because the rate constants are the same for each concentration of GoX. All experiments were done at approximately pH 9.5. Although the GoX stock solution was buffered at pH 7 (phosphate buffer) the colloid solutions were not buffered.

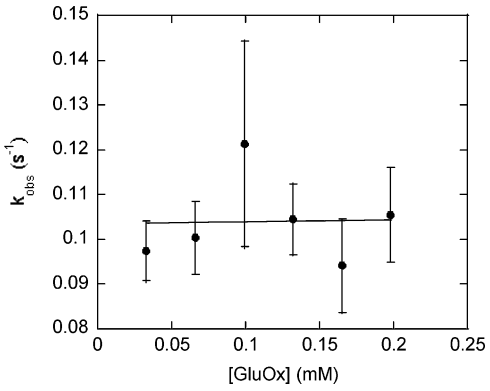

Figure 11. First-order rate constant determined by the fits to the data in Figure 10 are graphed against the concentration of GoX. The error bars represent the standard deviation over 3 trials.

The NHSS peak at 1780 cm^{-1} was also monitored for each GoX concentration. Figure 10 shows a representative graph of the intensity of the peak versus time for one GoX concentration.

An exponential regression analysis provided the first-order rate constants (k_{obs}) for each concentration of glucose oxidase investigated.

Figure 11 shows that the rate at which the active sites (NHSS ester) disappear is not dependent on the concentration of glucose oxidase. However, the rate of disappearance of the NHSS peak at 1780 cm^{-1} with a glucose oxidase concentration of 0.1 mM was found to depend linearly on the hydronium ion concentration and the results are shown in Figure 12. The possible base hydrolysis of the NHSS ester at pH 9.5 was ruled out by monitoring the NHSS peak when no glucose oxidase was present in solution. No change in the signal intensity at 1780 cm^{-1} was observed over 5 min when no glucose oxidase was present in solution.

The results obtained from this investigation are consistent with the kinetic model shown in Scheme 4, where *GoX* is glucose oxidase, *S−NHSS* is the NHSS bound to the surface, and S^+ represents an acylium ion on the surface. The S_N1-like mechanism explains why the disappearance of the NHSS peak

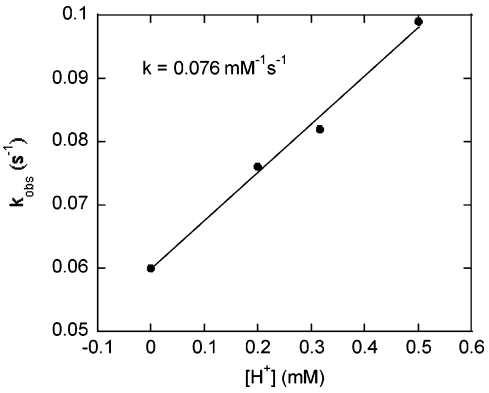

Figure 12. Dependence of k_{obs} to $[H^+]$ for a [GoX] = 0.1 mM. The closed circles represent the value of k_{obs}. The solid line through the data is the best-fit line with slope = $k_+ = 0.076$ $mM^{-1}s^{-1}$.

SCHEME 4: GoX Substitution Mechanism

$$H^+ + S-NHSS \underset{k_-}{\overset{k_+}{\rightleftarrows}} S^+ + NHSS$$

$$S^+ + GoX \xrightarrow{k} SGoX + H^+$$

does not depend on the concentration of GoX as show in Figure 7, but does depend on the pH as shown in Figure 12.

The integrated rate law predicted by the model was compared to the data in Figures 8−12. The intensity of the 980 cm^{-1} peak shown in Figure 8 corresponds to the rate of formation of *SGoX*. Equation 4 shows the predicted rate of appearance of this peak.

$$\frac{d\theta}{dt} = k(1 - \theta - \theta_{NHSS})[GoX] \quad (4)$$

In eq 1, $(1 - \theta - \theta_{NHSS})$ represents the fraction of open surface sites available for reaction with GoX. The rate of appearance of S^+ can be written as shown in eq 5.

$$\frac{d(1 - \theta - \theta_{NHSS})}{dt} = k_+[H^+]\theta_{NHSS} - k_-(1 - \theta - \theta_{NHS})[NHSS] - k(1 - \theta - \theta_{NHSS})[GoX] \quad (5)$$

Applying the steady-state approximation to S^+, eq 5 can then be solved for $(1 - \theta - \theta_{NHSS})$. Substitution of $(1 - \theta - \theta_{NHSS})$ into eq 4 gives

$$\frac{d\theta}{dt} = \frac{kk_+[H^+][GoX](1 - \theta)}{k_-[NHSS] + k_+[H^+] + k[GoX]} = k_{obs}(1 - \theta) \quad (6)$$

Thus, the model predicts an exponential increase in the coverage of GoX (θ), as shown in Figure 8. In the limit that, $k_+[H^+] \gg (k[GoX] + k_-[NHSS])$, $k_{obs} = k[Gox]$ and the linear dependence of k_{obs} is predicted to be directly proportional to *[GoX]* as observed in Figure 9.

The rate of disappearance of the peak at 1780 cm^{-1} is related to the rate of disappearance of the active site (θ_{NHSS}) on the colloid. The model predicts that the rate of disappearance of the active site is

$$\frac{-d\theta_{NHS}}{dt} = k_+[H^+]\theta_{NHS} - k_-[NHSS](1 - \theta - \theta_{NHSS}) \quad (7)$$

Substitution of the steady-state approximation for $(1 - \theta - \theta_{NHSS})$ into eq 7 yields eq 8 after simplification.

$$\frac{-d\theta_{NHSS}}{dt} = \frac{k[GoX]k_+[H^+]\theta_{NHSS}}{k_-[NHSS] + k[Gox]} = k'_{obs}\theta_{NHSS} \quad (8)$$

Thus, the model predicts an exponential decrease in the NHSS peak height, as observed in Figure 10. In the limit that $k_{-}[NHSS] \ll k[GoX]$, $k'_{obs} = k_{+}[H^{+}]$, and the linear dependence of k'_{obs} is predicted to be directly proportional to $[H^{+}]$ as observed in Figure 12.

Though this model is consistent with the results obtained, further work to verify this unexpected mechanism is necessary.

Conclusions

We present here recent progress in understanding the carbodiimide (EDC) coupling reaction to form an active N-hydroxysulfosuccinimde (NHSS) ester tethered to the surface of silver colloids. This reaction proceeds with mixed second-order kinetics consistent with a rate-limiting formation of the EDC adduct followed by fast reaction with NHSS.

Further reaction of the surface-immobilized active ester with a small nucleophile (histidine) and with a larger protein (glucose oxidase) has also been investigated. This reaction sequence is used extensively by many groups to covalently attach proteins to surfaces. Our investigation shows that the reaction of the active ester with a small molecule such as histidine proceeds with simple S_N2 kinetics. However, the reaction of the surface-immobilized active ester with a large protein such as glucose oxidase is by no means simple and has kinetics that are consistent with the formation of an intermediate acylium ion on the surface. The surprising results presented here point out the need to better understand a wider variety of surface reactions from a kinetic and mechanistic point of view. Broadening our understanding of important surface reactions should aid in development of simple routes to complex surface architectures.

Materials and Methods

Silver Colloid Solutions. Silver colloid solutions were made by the reduction of silver nitrate with hydrazine according to the literature.[32] Silver nitrate and hydrazine hydrochloride were purchased from Aldrich Chemicals and used without purification. A 0.300 mM solution of silver nitrate and a 0.375 mM solution of hydrazine hydrochloride were made volumetrically. The hydrazine hydrochloride solution was adjusted to a pH of 10.8. These solutions were mixed in a 1:1 ratio in small (40 mL) batches with stirring. The solution turned a clear yellow within seconds of mixing. Solutions were allowed to stir for approximately 1 h and then were combined to make a stock solution of silver colloids. To ensure clean, thiol-free colloids, all glassware used to make the colloid solutions was soaked in a 2% bleach solution and rinsed with copious amounts of distilled water. The glassware was than further purified by an E-pure filter and a deionization system.

Formation of Selfassembled Monolayers. A previous study by our group showed that these colloid solutions are saturated by approximately 18 μM concentrations of alkyl or aryl thiols. An 18-mL aliquot of 1 mM solution of 4-mercaptobenzoic acid (4MBA) (Aldrich) was delivered to a plastic 1-L storage bottle that had been cleaned in bleach. The chloroform was evaporated and 1 L of colloid solution was added to the storage bottle. This mixture was stirred at about 40 °C overnight. This procedure produced reproducible Raman scattering spectra without further treatment. The 4MBA saturated colloids were aggregated by lowering the pH to 3 using 0.50 M HCl. This solution was subsequently returned to a pH of about 7 using 0.50 M NaOH. A similar procedure was used to form monolayers of 16-mercaptohexadecanoic acid (MHDA) (Aldrich) except that the colloids were not aggregated prior to use. These stock colloid solutions were stable for over 3 months.

Kinetic Studies. *Formation of NHSS Ester*. A 10 mM stock solution of 1-[3-(Dimethylamino)propyl]-3-ethylcarbodiimide hydrochloride (EDC) (Aldrich) and a 100 mM stock solution of N-hydroxysulfosuccinimde sodium salt (NHSS) (Fluka) were prepared in water. These solutions were used over a two-to-three-day period and were kept refrigerated when not in use. Various volumes of stock solutions and water were mixed in small 1-mL vials to make a total volume of 50 μL. This was placed in the sample holder of the Detection Limit Solution-633 Raman spectrometer. A 950-μL aliquot of stock 4MBA colloid solution was added to the vial as the spectrometer was initiated. Between 3 and 5 spectra were averaged using an integration time of 3 s providing a data point every 9 to 15 s. The NHSS and EDC solutions were mixed just prior to each run since mixing these solutions in advance was shown to affect the results. The NHSS presumably reacts with the EDC, resulting in a lower EDC and NHSS concentration by the time the run is initiated.

Reaction of NHSS Ester with Histidine. A stock solution of 100 mM histidine in pH 7.0 phosphate buffer was prepared. Various volumes of this solution were added to a 4MBA colloid solution that had been incubated for 3−5 min with 1 mM NHSS and 0.5 mM EDC. Formation of the NHSS ester peak at a 1780 cm^{-1} Raman shift was verified before the addition of histidine. Between 2 and 5 spectra were averaged using an integration time of 3 s.

Reaction of NHSS Ester with Glucose Oxidase. A stock solution of 65 mg/mL of glucose oxidase from *Aspergillus niger* (Sigma Chemicals) in pH 7.0 phosphate buffer was prepared. Various volumes of this solution were added to a MHDA-saturated colloid solution that had been incubated for 3−5 min with 1 mM NHSS and 0.5 mM EDC. Formation of the NHSS ester peak at a 1780 cm^{-1} Raman shift was verified before the addition of glucose oxidase. One spectrum (integration time of 6 s) was obtained every 6 sec until the reaction was complete.

Acknowledgment. The authors acknowledge Allegheny College and the National Science Foundation for support of this research through NSF grant CHE-0094392.

References and Notes

(1) Scouten, W. H.; Luong, J. H. T.; Brown, S. R. *Tibtech* **1995**, *13*, 178.
(2) Ostuni, E.; Yan, L.; Whitesides, G. M. *Colloids Surf., B:* **1999**, *15*, 3.
(3) Ferretti, S.; Paynter, S.; Russell, D. A.; Sapsford, K. E.; Richardson, D. *J. Trends Anal. Chem.* **2000**, *19*, 530.
(4) Chechik, V.; Crooks, R. M.; Stirling, C. J. M. *Adv. Mater.* **2000**, *16*, 1161.
(5) Okuso, H.; Kurihara, K.; Kunitake, T. *Langmuir* **1994**, *10*, 3577.
(6) Lee, S.; Anzai, J.; Osa, T. *Bull. Chem. Soc. Jpn.* **1991**, *64*, 2019.
(7) Fryxell, G. E.; Rieke, P. C.; Wood, L. L.; Englehard, M. H.; Williford, R. E.; Graff, G. L.; Campbell, A. A.; Wiacek, R. J.; Lee, L.; Halverson, A. *Langmuir* **1996**, *12*, 5064.
(8) Templeton, A. C.; Hostetler, M. J.; Kraft, C. T.; Royce, M. W. *J. Am. Chem. Soc.* **1998**, *120*, 1906.
(9) Van Ryswyk, H.; Turtle, E. D.; Watson-Clark, R.; Tanzer, T. A.; Herman, T. K.; Chong, P. Y.; Waller, P. J.; Taurog, A. L.; Wagner, C. E. *Langmuir* **1996**, *12*, 6143.
(10) Caruso, F.; Rodda, E.; Furlong, D. N. *J. Colloid Interface Sci.* **1996**, *178*, 104.
(11) Guiomar, A. J.; Guthrie, J. T.; Evans, S. D. *Langmuir* **1999**, *15*, 1198.
(12) Willner, I.; Lapidot, N.; Riklin, A.; Kasher, R.; Zahavy, E.; Katz, E. *J. Am. Chem. Soc.* **1994**, *116*, 1428.
(13) Tatsuma, T.; Tsuzuki, H.; Okawa, Y.; Yoshida, S.; Wtatnabe, T. *Thin Solid Films* **1991**, *202*, 145.
(14) Anzai, J.; Lee, S.; Osa, T. *Chem. Pharm. Bull.* **1989**, *37*, 3320.
(15) Karymov, M. A.; Kruchinin, A. A.; Tarantov, Yu. A.; Balova, I. A.; Remisova, L. A.; Sukhodolov, N. G.; Yanklovich, A. I.; Yorkin, A. M. *Sens. Actuators, B* **1992**, *6*, 208.

(16) Gregorius, K.; Mouritsen, S.; Elsner, H. I. *J. Immunological Methods* **1995**, *181*, 65.
(17) Willner, I.; Riklin, A. *Anal. Chem.* **1994**, *66*, 1535.
(18) Hamachi, I.; Noda, S.; Kunitake, T. *J. Am. Chem. Soc.* **1990**, *112*, 6744.
(19) Decher, G. *Science* **1997**, *277*, 1232.
(20) Lvov, Y. M.; Lu, Z.; Schenkman, J. B.; Zu, X.; Rusling, J. F. *J. Am. Chem. Soc.* **1998**, *120*, 4073.
(21) Firestone, M. A.; Shank, M. L.; Sligar, S. G.; Bohn, P. W. *J. Am. Chem. Soc.* **1996**, *118*, 9033.
(22) Samuelson, L. A.; Kaplan, D. L.; Lim, J. O.; Kamath, M.; Marx, K. A.; Tripathy, S. K. *Thin Solid Films* **1994**, *242*, 50.
(23) Sigal, G. B.; Bamdad, C.; Barberis, A.; Strominger, J.; Whitesides, G. M. *Anal. Chem.* **1996**, *68*, 490.
(24) Owaku, K.; Goto, M.; Ikariyama, Y.; Aizawa, M. *Anal. Chem.* **1995**, *67*, 1613.
(25) Lahiri, J.; Isaacs, L.; Grzybowski, B.; Carbeck, J. D.; Whiteside, G. M. *Langmuir* **1999**, *15*, 7186.
(26) Reichert, A.; Nagy, J. O.; Spevak, W.; Charych, D. *J. Am. Chem. Soc.* **1995**, *117*, 829.
(27) Kneipp, K.; Kneipp, H.; Itzkan, I.; Dasari, R. R.; Feld, M. S. *Chem. Rev.* **1999**, *99*, 2957.
(28) Creighton, J. A. In *Surface Enhanced Raman Scattering*; Change, R. K., Furtak, T. E., Eds.; Plenum Press: New York, 1982; p 315.
(29) Evans, D. F.; Wennerstrom, H. *The Colloidal Domain: Where Physics, Chemistry, and Biology Meet*, 2nd ed.; Wiley-VCH: New York, 1999; Chapter 2.
(30) Li, X.; Zhang, J.; Xu, W.; Jia, H.; Wang, X.; Yang, B.; Zhao, B.; Li, B.; Ozaki, Y. *Langmuir* **2003**, *19*, 4285.
(31) Mandal, S.; Gole, A.; Lala, N.; Gonnade, R.; Ganvir, V.; Sastry, M. *Langmuir* **2001**, *17*, 6262.
(32) Nickel, U.; zu Castell, A.; Poppl, K.; Schneider, S. *Langmuir* **2000**, *16*, 9087.